Antimicrobial, Antioxidant, and Waterproof RTV Silicone-Ethyl Cellulose Composites Containing Clove Essential Oil

José A. Heredia-Guerrero[1], Luca Ceseracciu[2], Susana Guzman-Puyol[1], Uttam C. Paul[1], Alejandro Alfaro-Pulido[1], Chiara Grande[3], Luigi Vezzulli[3], Tiziano Bandiera[4], Rosalia Bertorelli[4], Debora Russo[4], Athanassia Athanassiou[1*], Ilker S. Bayer[1*]*

[1]Smart Materials, Istituto Italiano di Tecnologia, Via Morego 30, Genova, 16163, Italy.

[2]Materials Characterization Facility, Istituto Italiano di Tecnologia, Via Morego 30, Genova, 16163, Italy.

[3]Department of Earth, Environmental, and Life Sciences, University of Genova, 16132 Genova, Italy.

[4]D3-Pharma Chemistry, Drug Discovery and Development, Istituto Italiano di Tecnologia, Via Morego, 30, Genova, 16163, Italy.

*Corresponding authors: jose.heredia-guerrero@iit.it, athanassia.athanassiou@iit.it, ilker.bayer@iit.it

Abstract

Ethyl cellulose (EC) / polydimethylsiloxane (PDMS) composite films were prepared at various concentrations of PDMS in the films (0, 5, 10, 15, and 20 wt.%). Morphological and chemical analysis by EDX-SEM and ATR-FTIR showed that EC-rich matrices and PDMS-rich particles were formed, with the two polymers interacting through H-bonds. The number and diameter of particles in the composite depended on the PDMS content and allowed a fine tuning of several properties such as opacity, hydrophobicity, water uptake, and water permeability. Relative low amounts of clove essential oil were also added to the most waterproof composite material (80 wt.% ethyl cellulose and 20 wt.% PDMS). The essential oil increased the flexibility and the antioxidant capacity of the composite. Finally, the antimicrobial properties were tested against common pathogens such as *Escherichia coli*, *Staphylococcus aureus* and *Pseudomonas aeruginosa*. The presence of clove essential oil reduced the biofilm formation on the composites.

Keywords: ethyl cellulose, PDMS, clove essential oil, composite, waterproofing, food packaging.

1.- Introduction

Ethyl cellulose (EC) is a cellulose derivative, where some hydroxyl groups of the cellulose backbone are substituted by ethyl ether groups. It is usually synthesized from sodium hydroxide solutions of wood pulp in the presence of ethyl chloride (Wüstenberg, 2014). EC is a versatile material with many interesting properties, *e.g.* it is a thermoplastic (melting point range 240-255°C), non-toxic, and edible polymer (Cerqueira, Pereira, da Silva Ramos, Teixeira, & Vicente, 2016). It is soluble in common organic solvents but insoluble in water and is compatible with some other synthetic polymers, fillers and plasticizers (Davidovich-Pinhas, Barbut, & Marangoni, 2014; Murtaza, 2012). It also forms robust films when cast from organic solvents. Due to these characteristics, EC is used as additive and excipient in drug formulations, cosmetics, and food technology (Davidovich-Pinhas et al., 2014). However, EC has a high glass transition temperature (~143^{o}C) that needs to be reduced by plasticizer addition in order to improve flexibility at room temperature. Common plasticizers for EC are diethyl phthalate, dibutyl sebacate, and triethyl citrate (Hyppölä, Husson, & Sundholm, 1996), although other nontraditional plasticizers with bioactive applications, such as ibuprofen (a common pain killer), have also been very effective (de Brabander, van den Mooter, Vervaet, & Remon, 2002). Interestingly, the necessary amount of plasticizer to achieve the desired degree of softening corresponds to 15-20 wt.% with respect to EC polymer, while other common cellulose derivatives such as nitrocellulose or cellulose acetate require higher percentages close to 30-35 wt.% (Wüstenberg, 2014). These plasticizers are usually low molecular weight compounds that can easily migrate and leach from polymer matrix, inducing polymer rigidity over time and negatively affecting the desired application (Rahman & Brazel, 2004). To avoid this problem, different strategies, such as compositing with other polymers, have been used. Polymer particles can modify the mechanical properties of composites and do not leach away due to low diffusion of solid macromolecules in the polymer host (Hammer, 1978). In particular, for instance, EC biocomposites have been prepared with polyvinylpyrrolidone, zein, or poly(3-hydroxybutyrate) (Chan, Ong, & Heng, 2005; Iqbal, Kyazze, Locke, Tron, & Keshavarz, 2015; Lu, Wang, Li, Qiu, & Wei, 2017). On the other hand, recent works demonstrated that polydimethylsiloxane (PDMS) can strongly interact with polysaccharides (*e.g.*, starch, cellulose or polysaccharide-rich materials, such as red beetroot or cocoa shells wastes) by formation of hydrogen bonds (Ceseracciu, Heredia-Guerrero, Dante, Athanassiou, & Bayer, 2015; Tran, Athanassiou, Basit, & Bayer, 2017; Tran, Heredia-Guerrero, et al., 2017; Zahid, Heredia-Guerrero, Athanassiou, & Bayer, 2017). Combination of EC and PDMS (as non-crosslinked viscous liquid) with other plasticizers such as di-*n*-butylphthalate, centchroman, and propylene glycol have been used for the fabrication of transdermal patches (Gupta et al., 2016). PDMS is the major component or precursor of siloxane elastomers that are commercially produced with good hydrophobicity, tunable elasticity,

and high thermal, light, and chemical stability (Esteves et al., 2009). It has also been approved as food additive (Jamuna, 2010). Furthermore, PDMS can biodegrade in soil by abiotic hydrolysis, microbiotic degradation, and volatilization (Lukasiak, Dorosz, Prokopowicz, Rosciszewski, & Falkiewicz, 2005). In order to transform viscous PDMS liquids into soft but robust solid elastomeric networks, they need to be crosslinked. There are several crosslinking or curing pathways, such as peroxide-initiated free radical reactions activated by heat, condensation reactions taking place in the presence of a tin salt or titanium alkoxide catalyst, Room Temperature Vulcanizing (RTV) moisture cure and addition reactions that are generally catalyzed by a platinum or rhodium complex, and not excluding photo-initiated curing systems as well (Mashak & Rahimi, 2009). Among these, PDMS oligomers that can be crosslinked in the presence of acetoxy-silanes via RTV moisture cure process are highly suitable for combining with polysaccharides, since the polymerization can be initiated by the naturally adsorbed superficial water as well as ambient moisture at room temperature (Ceseracciu et al., 2015).

Blends of EC with essential oils from diverse plants such as clove, fennel, rosemary, caraway, cinnamon, lemongrass, or eucalyptus have been intensely investigated for the fabrication of antimicrobial or insect repellent packaging materials and wound dressings (Badulescu, Vivod, Jausovec, & Voncina, 2008; Chattopadhyay et al., 2015; Kwiatkowski, Giedrys-Kalemba, Mizielińska, & Bartkowiak, 2016; Patil, Agrawal, Mahire, & More, 2016). Among the different essential oils, clove essential oil, mainly composed by eugenol and extracted from the plant *Syzygium aromaticum*, is commercially available and displays significant multifunctional bioactivity such as antimicrobial, antioxidant, antifungal, and antiviral activity as well as anti-inflammatory, cytotoxic, insect repellent, and anesthetic properties (Chaieb et al., 2007). It is used in food processing and packaging as an additive (CAS number 8000-34-8) in order to extend the shelf life of perishables (Burt, 2004; Matan et al., 2006). It is also known for its antimicrobial and antioxidant properties (Burt, 2004; Chaieb et al., 2007). All these characteristics are important for food packaging materials (Biji, Ravishankar, Mohan, & Srinivasa Gopal, 2015).

Hence, in this work, we combine EC with acetoxy-RTV PDMS silicones in ethyl acetate to produce soft, flexible and waterproof cellulose-derived plastics. Further, we demonstrate that incorporation of clove essential oil not only confers to the plastics antioxidant and antibacterial activity but also improves flexibility for potential food packaging applications. We finally demonstrate the antimicrobial efficacy of the resultant composite materials by *in vitro* biofilm inhibition tests against Gram-negative (*E. coli*) and Gram-positive (*S. aureus* and *P. aeruginosa*) bacterial strains.

2.- Material and methods

2.1.- Materials

Ethyl cellulose (48% ethoxyl, viscosity 22cP for a solution 5% in toluene/ethanol 80:20), 2,2-diphenyl-1-picrylhydrazyl radical (DPPH·), ethanol (purity ≥99.5%), and ethyl acetate (purity ≥99.5%) were purchased from Sigma-Aldrich and used without further purification. Acetoxy-polydimethylsiloxane (acetoxy-PDMS, Elastosil E43) was obtained from Wacker Chemie AG, Germany. Elastosil E43 is a patented mixture of hydroxyl-terminated polydimethylsiloxane (PDMS) and triacetoxymethylsilane. Clove essential oil was kindly provided by Plant Lipids Company (India).

Two reference Gram-negative bacterial strains (*Escherichia coli* ATCC 25404 and *Pseudomonas aeruginosa* ATCC 27853) and one Gram-positive strain (*Staphylococcus aureus* ATCC 29813) were used for biofilm studies. Bacterial strains were obtained from American Type Culture Collection (ATCC®). All the strains were cultured in Mueller Hinton Broth (MHB) at 37°C.

2.2.- Preparation of the composites

EC:PDMS composite films were prepared by mixing ethyl cellulose and PDMS solutions in ethyl acetate. Ethyl cellulose solutions with a concentration of 0.1 g/mL were prepared by dissolving ethyl cellulose powder in ethyl acetate. The complete dissolution occurred after 1.5 h at room conditions. Similar solutions were prepared with silicone monomers (Elastosil E43) in ethyl acetate. PDMS precursors dissolved in 15 minutes. Films were prepared by mixing predetermined volumes of the above solutions in order to obtain various concentrations of PDMS in the films, namely 0, 5, 10, 15, and 20 wt.%. Percentages higher than 20 wt.% resulted in macroscopic segregation of both components. Clove essential oil was directly added to the blended solutions of EC and PDMS (in particular to 80 wt.% EC and 20 wt.% PDMS) at different percentages of the total amount of polymer (0, 1, 5, and 10 wt.%). A control sample of pure PDMS was also prepared following the same procedure. The solutions were drop-casted on glass Petri dishes and the solvent was evaporated under an aspirated hood for 24 h. A graphical presentation of composite preparation is shown in Figure 1A for visual clarity. Composites were labeled as EP0 (pure ethyl cellulose), EP5, EP10, EP15, and EP20 according to the PDMS content. When clove essential oil was added to the EP20 solutions, composites were labeled as EPC0 (same as EP20), EPC1, EPC5, and EPC 10 according to the clove essential oil content. All samples were stored at 44% RH for few days before analysis to ensure the polymerization of PDMS precursors.

2.3.- Characterization

125 The morphology of the composites was characterized by scanning electron microscopy (SEM), using
126 a JEOL JSM-6490LA microscope working in high vacuum mode, with an acceleration voltage of 15
127 kV. The diameter (as a result of phase separation) and surface density of the particles were calculated
128 by using the software ImageJ. Compositional SEM images were used to measure both diameter and
129 number of particles. The images were loaded into the software and the particles' diameter was
130 measured using a two point measuring analysis. For the particle count, highly contrasted images were
131 used. Approximately 100 measurements were taken to obtain each diameter and density distributions.
132 Energy dispersive X-ray analysis (EDX) was also conducted during SEM imaging in order to
133 investigate the presence of chemical elements in the different composites.

134 Infrared spectra were obtained with a single-reflection attenuated total reflection (ATR) accessory
135 (MIRacle ATR, PIKE Technologies) coupled to a Fourier Transform Infrared (FTIR) spectrometer
136 (Equinox 70 FT-IR, Bruker). All spectra were recorded in the range from 3800 to 600 cm^{-1} with a
137 resolution of 4 cm^{-1}, accumulating 128 scans. To assess the homogeneity of chemical composition,
138 ATR-FTIR spectra were repeated in three different areas.

139 Opacity was determined by measuring the film absorbance at 600 nm using a UV spectrophotometer
140 Varian Cary 6000i. Films were cut into rectangle pieces and directly placed in the spectrophotometer
141 test cell. An empty test cell was used as the reference. The opacity of films was calculated by the
142 following equation as previously reported (Heredia-Guerrero et al., 2017):

143 $$Opacity = \frac{A_{600}}{x}$$

144 where A_{600} is the value of absorbance at 600 nm and x is the film thickness (mm).

145 Mechanical properties of the films were measured by uniaxial tensile tests on a dual column Instron
146 3365 universal testing machine. Dog-bone shaped samples were stretched at a rate of 10 mm/min. All
147 the stress-strain curves were recorded at 25°C and 44% RH. Ten measurements were conducted for
148 each sample and the results were averaged to obtain a mean value. The Young's modulus and the
149 stress and elongation at break values were calculated from the stress-strain curves.

150 To characterize the surface wettability, water static contact angles (W-CA) were measured with the
151 sessile drop method at room temperature at ten different locations on each surface using a contact
152 angle goniometer (DataPhysics OCAH 200). Three μL droplets of milli-Q water were deposited on
153 the surfaces and side view images of the drops were captured. W-CAs were automatically calculated
154 by fitting the captured drop shape. W-CAs were measured after 2 min from drop deposition on the
155 surface in order to consider values at equilibrium.

The water vapor permeability (WVP) of films was determined at 25ºC and under 100% relative humidity gradient (ΔRH %) according to the ASTM E96 standard method. 400 µL of deionized water (which generates 100% RH inside permeation cell) was placed in each test permeation cell with a 4 mm inner diameter and a 10 mm inner depth. Films were cut into circles and mounted on the top of the permeation cells. The permeation cells were placed in 0% RH desiccator with anhydrous silica gel as a desiccant agent. The water transferred through the film was determined by the weight change of the permeation cell every hour during the first 8 h using an electronic balance (0.0001 g accuracy). The weight loss of the permeation cells was plotted as a function of time. The slope of each line was calculated by linear fitting. Then, the water vapor transmission rate (WVTR) was determined as below (Ho, Zimmermann, Ohr, & Caseri, 2012):

$$WVTR\ (g/(m^2 \cdot day)) = \frac{Slope}{Area\ of\ the\ film} \quad (1)$$

WVP measurements were replicated three times for each film. The WVP of the film was calculated as follows:

$$WVP\ (g/(m \cdot day \cdot Pa)) = \frac{WVTR \times l \times 100}{p_s \times \Delta RH} \quad (2)$$

where, l (m) is the film thickness, measured with a micrometer with 0.001 mm accuracy, ΔRH (%) is the percentage relative humidity gradient, and p_s (Pa) is the saturation water vapor pressure at 25ºC (3168 Pa).

Water uptake measurements were carried out as follows: dry samples were weighed (~30 mg) on a sensitive electronic balance and then they were placed in different chambers with increasing humidity. Samples were dried by conditioning in a desiccator until no change in sample weight was measured. The humidity conditions were 0% and 100%. After conditioning in different humidity chambers until equilibrium conditions, each film was weighed and the amount of adsorbed water was calculated based on the initial dry weight as the difference.

The antioxidant capacity of the samples was determined by using the standard DPPH• free radical scavenging method according to the procedure described elsewhere (Brandwilliams, Cuvelier, & Berset, 1995). The method is based on the scavenging of DPPH radical through the action of an antioxidant that decolorizes the DPPH solution. Briefly, 5x5 mm^2 films were added to 3 mL of 0.1 mM DPPH solution in ethanol. The decrease in absorbance was determined at 515 nm with a Cary JEOL spectrophotometer at different times. All the measurements were performed in triplicate and

the results were averaged to obtain a mean value. Radical scavenging activity was expressed as the inhibition percentage of free radical by the sample and calculated as follows:

$$Radical\ Scavenging\ Activity\ (\%) = \frac{A_0 - A_1}{A_0} * 100$$

where A_0 is the absorbance value of the control (3 mL of 0.1mM DPPH solution in ethanol) and A_1 is the absorbance value of the sample at different times.

For biofilm studies, two reference gram-negative bacterial strains (*Escherichia coli* ATCC 25404 and *Pseudomonas aeruginosa* ATCC 27853) and one gram-positive strain (*Staphylococcus aureus* ATCC 29213) were used. All the strains were obtained from American Type Culture Collection (ATCC®). For the microtiter plate biofilm inhibition assay, biofilms were cultured in 96-well tissue-culture-treated polystyrene microtiter plates (Corning Inc.). 6 mm diameter discs were cut from EC:PDMS (-/+ clove essential oil) composite films by a punch (Harris Uni-Core, Whatman) and put on the bottom of each well. Overnight cultures of all bacteria strains were centrifuged at 4500 rpm, rinsed with phosphate buffered saline (PBS, pH 7.4) two times and re-suspended in PBS to approximately 10^9 CFU/mL. Aliquots of cells (20 µL each) were transferred to the wells along with 180 µL of Mueller Hinton Broth (MHB), and the plate was incubated at 37°C for 24 h or 48 h. After incubation, the culture broth was carefully removed and the biofilms bound to the surface of the film were rinsed once with PBS and stained for 15 min at room temperature with 100 µL of 0.4% Gram's crystal violet solution (Sigma-Aldrich). Stained biofilms were rinsed with sterile deionized water and crystal violet was solubilized by incubating each well with 200 µL of absolute ethanol for 15 min at room temperature. The absorbance of the crystal violet solution was measured at 540 nm by using a spectrophotometer (Varian Cary 50 Bio, UV-Visible Spectrophotometer). Both films were tested in five replicates.

GraphPad Prism 5 was used for all statistical analysis (GraphPad Software Inc. San Diego, CA, USA). All values were expressed in terms of mean ± S.D. A one-way ANOVA followed by a Bonferroni's post hoc-test was applied for comparison of the test and control, with a *P* value of <0.05 considered as significant.

Percentages of biofilm inhibition by clove essential oil containing films were calculated using the following formula:

$$Biofilm\ inhibition = 100 - \left(\frac{EPC5\ A540}{EP20\ A540}\right) * 100$$

where *EPC5 A*540 is the absorbance measured for the biofilm growth on the EPC5 substrate and *EP20 A*540 is the absorbance measured for the biofilm growth on the EP20 substrate sample (which represents the 100% of the biofilm formed for each strain).

3.- Results and discussion

3.1.- Morphological and Chemical Characterization

Figure 1B shows photographs of the EC:PDMS films (EP samples). EP0 (pure ethyl cellulose) was transparent and colorless, while a white color was observed in the other samples (EP5, EP10, EP15, and EP20). The opacity of the samples was directly proportional to the PDMS content and ranged from ~0.3 a. u./mm for EP0 to ~8.3 a. u./mm for EP20, Figure 1C.

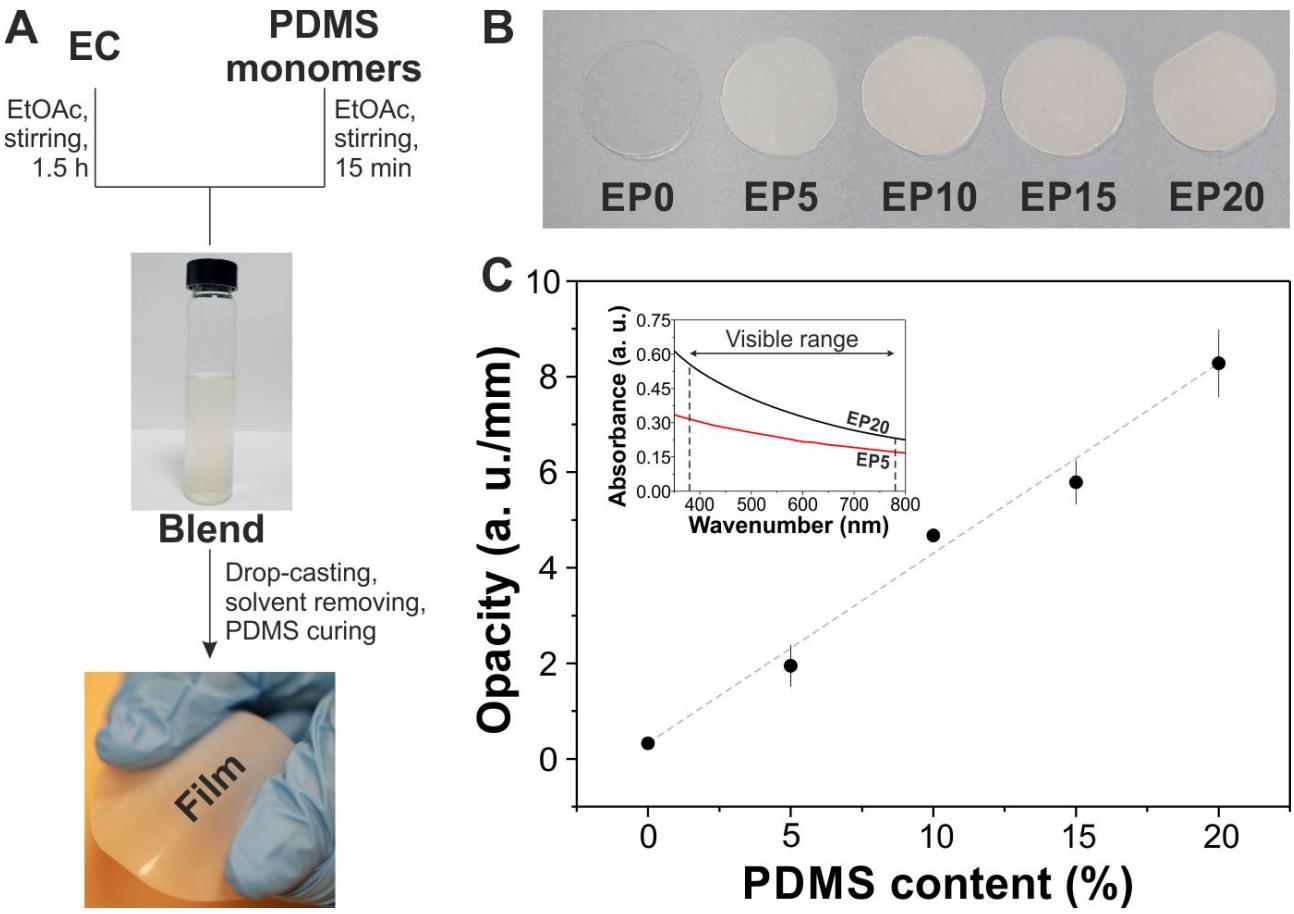

Figure 1. A, Schematic representation of the composite preparation. **B**, photographs of EP composite materials. **C**, variation of the opacity of EP composites with the content of PDMS. The inset shows the UV-vis spectra of EP5 and EP20 samples with the same thickness in the visible region.

The morphology of the composites was characterized by SEM. Topographic SEM images revealed very smooth and homogeneous surfaces as well as particles and cavities in the cross-section (Figure S1). The corresponding compositional SEM images, Figures 2A,B, show well defined sphere-like

particles of different diameters embedded in a continuous matrix. In particular, Figure 2B displays also the cavities that such particles form inside the host matrix. The EDX atomic signal distribution in the particles and the matrix are compared in Figure 2C. Both of them are composed of Si, C, and O, being the relative concentration of Si is much higher in the particles. The surface density of the particles (calculated as the number of particles in 100 μm^2) was determined from the compositional SEM images, as reported in Figure 2D. A linear growth of the surface density was observed for low PDMS contents while a plateau at ~32 particles/100 μm^2 was reached for EP15 and EP20 samples. In addition, the particle diameter was increased with the PDMS content, as graphed in Figure 2E. The increase in both surface density and particle diameter with the PDMS content can explain the higher opacity values measured for the samples richer in silicone.

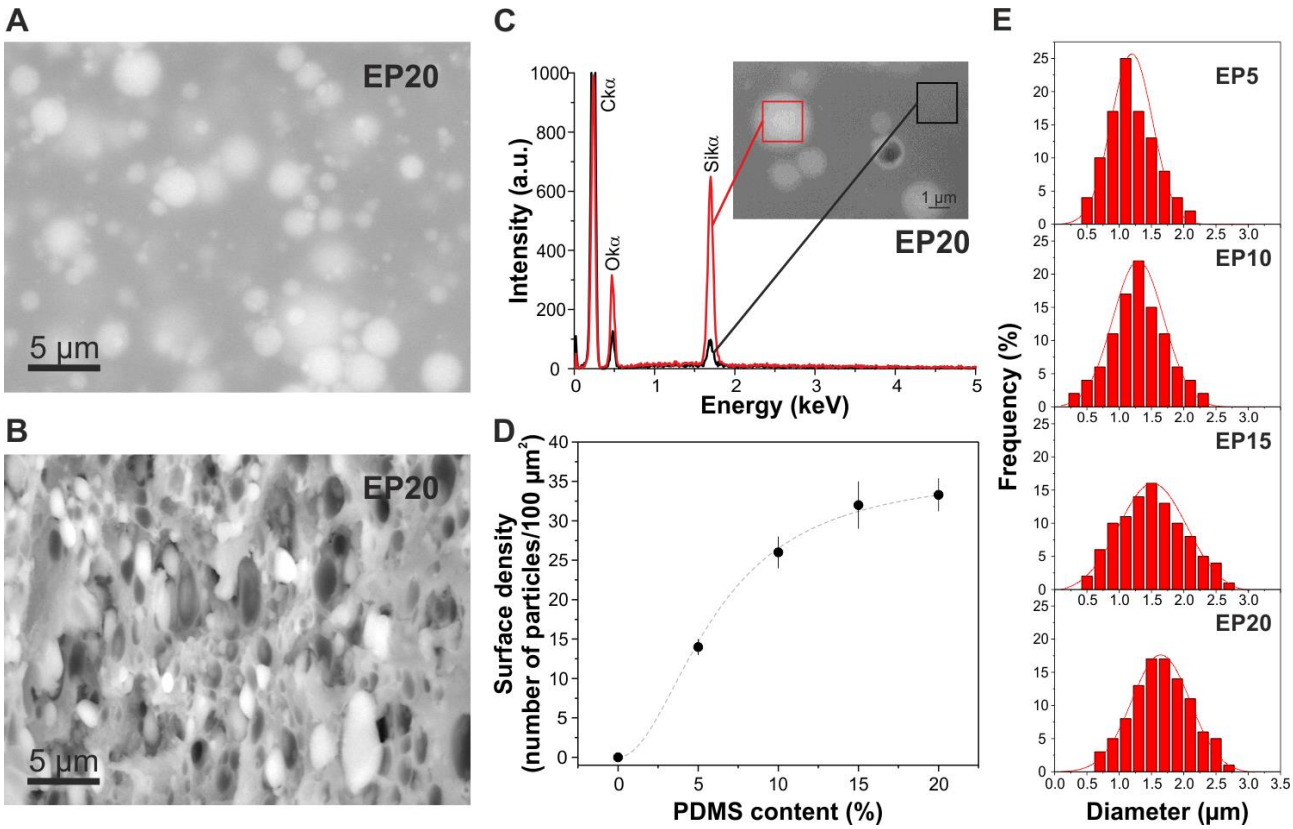

Figure 2. A, compositional SEM top-view of the EP20 sample. **B**, compositional SEM cross-section of the EP20 sample after a tensile test. The elongation of particles and their corresponding cavities can be caused by the tensile forces. **C**, EDX chemical analysis of the particles (red line) and the host matrix (black line) for the EP20 sample. **D**, surface density of particles in the composite as a function of the content of PDMS. **E**, Histograms showing the diameter distribution of the particles for EP5, EP10, EP15, and EP20 composites.

The chemical characterization of EP samples was carried out by ATR-FTIR. Figure 3A shows the infrared spectra of PDMS, EP0, EP10, and EP20 in the range between 3800 and 2700 cm^{-1}. The bands associated with PDMS (CH_3 asymmetric and symmetric stretching modes at 2962 and 2906 cm^{-1}, respectively) were masked for those of EC (O-H stretching mode at 3472 cm^{-1} and diverse C-H stretching modes in the 3000-2800 cm^{-1} region) in EP10 and EP20 (Elzein, Galliano, & Bistac, 2004; Laredo, Barbut, & Marangoni, 2011). At lower wavenumbers, Figure 3B, PDMS was characterized by the presence of different peaks at 1260 cm^{-1} (CH_3 symmetric bending mode), 1063 cm^{-1}, 1009 cm^{-1} (Si-O-Si symmetric and asymmetric stretching modes, respectively), and 796 cm^{-1} (CH_3 rocking mode), while for EP0 the peaks appeared in the 1500-1330 cm^{-1} region (different CH bending modes: deformation, rocking and wagging), at 1053 cm^{-1} (C-O-C stretching modes of the ethoxy groups and the glycosidic bond) and 919 cm^{-1} (C-C stretching mode) (Elzein et al., 2004; Laredo et al., 2011). The presence of PDMS bands in the composites' spectra was proportional to the silicone content. Furthermore, the CH_3 rocking mode of PDMS shifted 14 cm^{-1} from ~802 cm^{-1} for EP5 to ~788 cm^{-1} for pure PDMS, as illustrated in Figure 3C. The shift was linear in the range of PDMS content between 5% and 20% and attributed to the formation of H-bonds between the O-H groups of the polysaccharide and the oxygen of the siloxane groups of the cross-linked PDMS (Ceseracciu et al., 2015; Zahid et al., 2017), indicating that both components can interact by such secondary bonds in the composite.

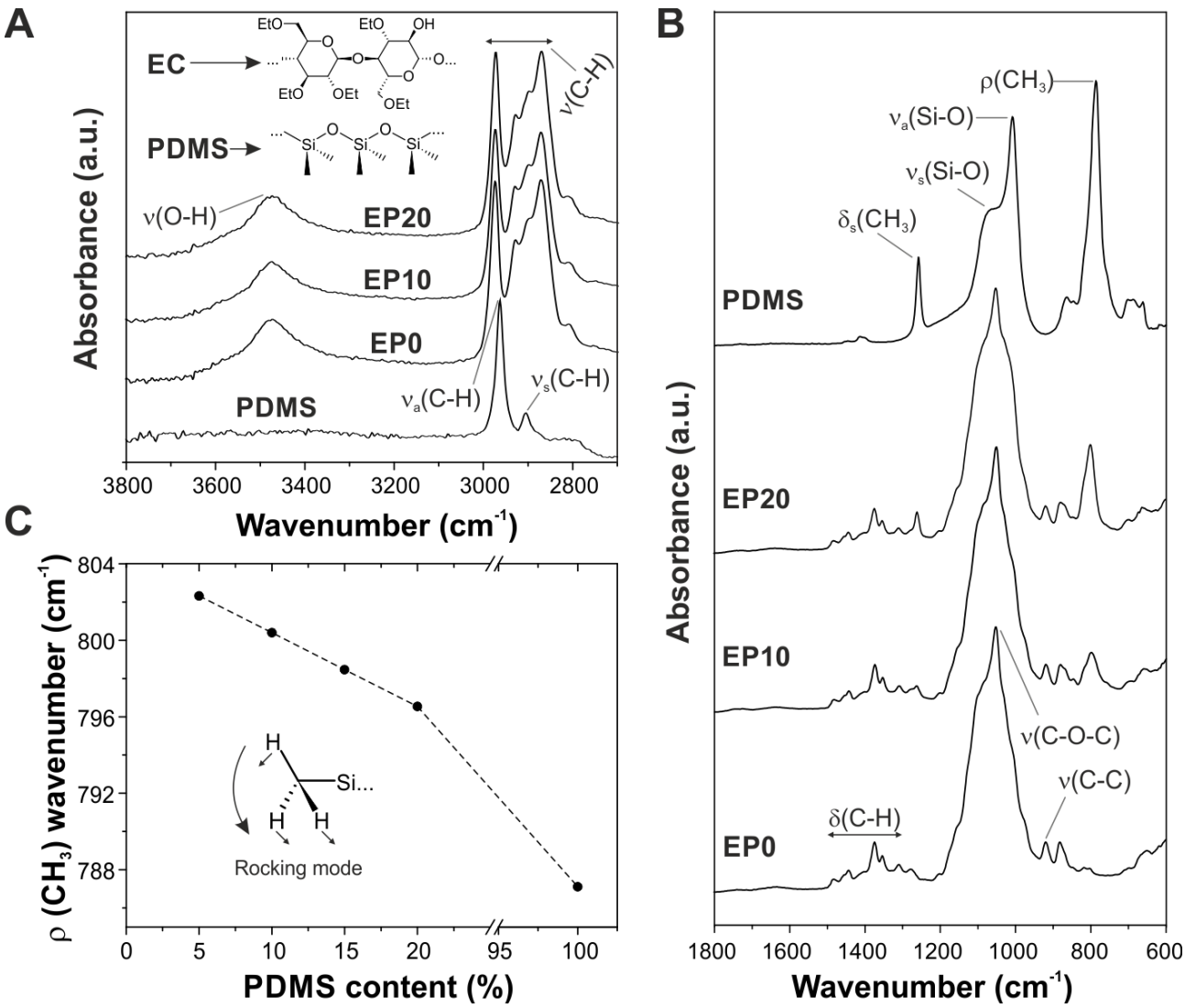

Figure 3. A, ATR-FTIR spectra of pure PDMS, EC0, EC10, and EC20 samples in the 3800-2700 cm^{-1} region. The chemical structures of EC and PDMS are included. **B**, ATR-FTIR spectra of pure PDMS, EC0, EC10, and EC20 samples in the 1800-600 cm^{-1} region. **C**, shift of the $\rho(CH_3)$ band. The rocking mode of PDMS methyl groups is shown.

3.2.- Mechanical characterization.

Stress-strain behaviour of the films (tensile tests) is reported in Figure 4. The response of all composites was typical of ductile materials, with a clear yield point and successive plastic deformation. The extent of the plastic regime became shorter with the addition of PDMS. Considering the mechanical parameters, the addition of PDMS initially did not considerably affect the Young's modulus with a value of *ca.* 1200 MPa, although a clear drop to ~750 MPa was visible at high concentration (20 wt.%) of filler. Strength and elongation at break values ranged from ~45.0 MPa to

~22.5 MPa and from 13.5% to 5.5%, respectively, with the decrease becoming more evident above 10 wt. % of PDMS concentration in the composites. This suggests that the soft PDMS-rich particles act as starting points for the onset of plastification and eventual fracture.

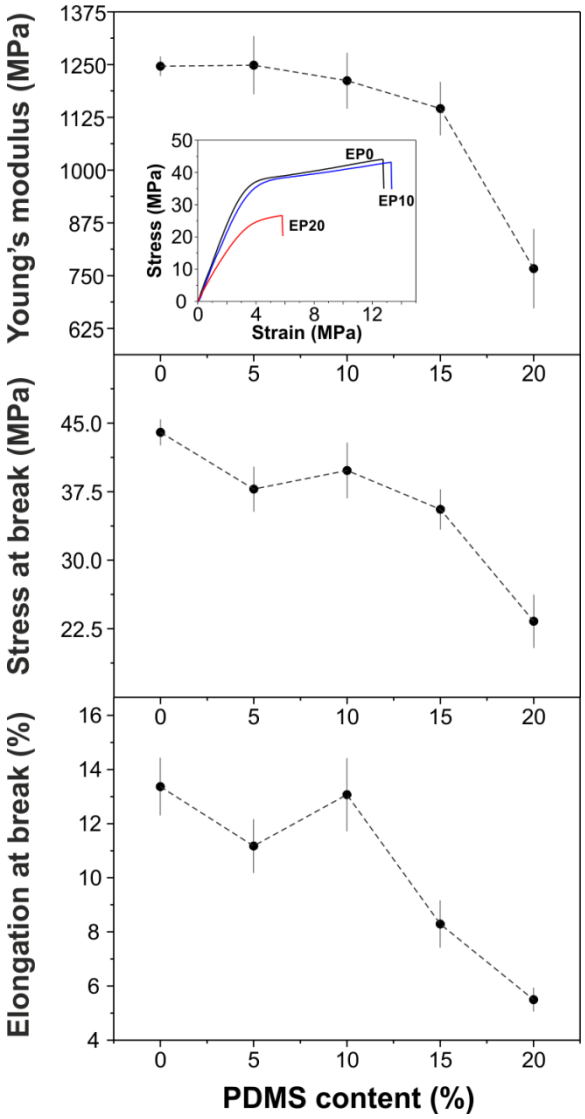

Figure 4. Variation of the Young's modulus, stress at break, and elongation at break with the content of PDMS. The inset shows the representative stress-strain curves of EC0, EC10, and EC20 samples.

3.3.- Wettability, Water Uptake, and Water Barrier Properties.

The water contact angle (WCA), water uptake, and water vapor permeability (WVP) data of the composites are shown in Figure 5. The WCA was increased from ~73° for EP0 to ~112° for EP20, most likely due to the inherent hydrophobic properties of PDMS with a WCA of value ~120° (Ceseracciu et al., 2015). On the other hand, water uptake values were in general very low, decreasing

from ~4% for pure EC to ~1.8% for EP20. Moreover, the WVP values were also decreased with the PDMS content. EP0 sample had a value of ~1.9 · 10^{-10} g m^{-1} s^{-1} Pa^{-1}, while for EP20 the water permeability was ~1.1 · 10^{-10} g m^{-1} s^{-1} Pa^{-1} (a reduction of ~42%). Interestingly, these values are very low when compared to those of common biopolymers used in food packaging such as cellulose acetate (2.3 · 10^{-5} g m^{-1} s^{-1} Pa^{-1}), polycaprolactone (1.4 · 10^{-6} g m^{-1} s^{-1} Pa^{-1}), poly(lactic acid) (6.5 · 10^{-7} g m^{-1} s^{-1} Pa^{-1}) or polyhydroxybutyrate-valerate copolymer (1.7 · 10^{-7} g m^{-1} s^{-1} Pa^{-1}) (Shogren, 1997). Such a reduction of water uptake and WVP is related to the water-repellent behavior of the silicone, the size and presence of hydrophobic PDMS-rich particles and to the participation of ethyl cellulose's OH groups in H-bonds with PDMS, which could reduce interaction with water molecules.

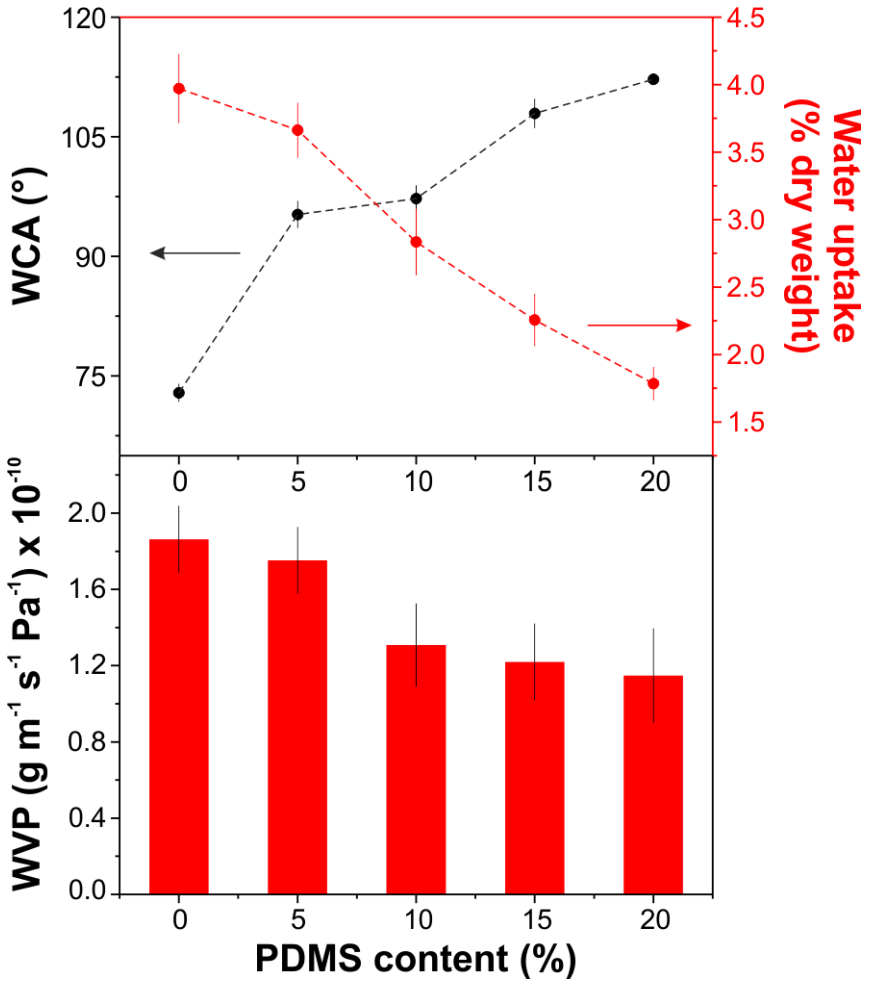

Figure 5. Water contact angle, water adsorption and water vapor permeability (WVP) as a function of the PDMS content.

3.4.- Effect of the clove essential oil on EC:PDMS composites.

The effect of the clove essential oil on the properties of EP20 sample, the composite with the best waterproofing properties, was studied. Figure 6A shows the infrared spectra of EP20, EPC1, EPC5,

and EPC10 in the 1650-1500 cm^{-1} region. Bands at 1638 cm^{-1} (C=C vinyl stretching mode), 1604 cm^{-1}, and 1515 cm^{-1} (both bands related to C=C aromatic stretching modes) were associated with the chemical structure of eugenol (Chowdhry, Ryall, Dines, & Mendham, 2015). The intensity of these bands increased with the clove essential oil content. No additional bands or shifts were detected in the rest of the analyzed spectral region. Furthermore, no important changes in the surface density and diameter of the PDMS-rich particles were observed. As a representative example of the composites with clove essential oil, a compositional SEM cross-section of the EPC5 sample is shown in Figure 6B. However, the tensile mechanical properties of the films were modified by the presence of the essential oil, as displayed in Figure 6C. Both Young's modulus and stress at break of samples increase for low clove essential oil concentration (1 wt.%), while for higher oil concentrations their values are lower than the initial values of EP20. On the contrary, the elongation at break is higher than the initial value of EP20 for all the essential oil concentrations. This indicates a plasticizer effect due to the oil that resulted in a higher flexibility.

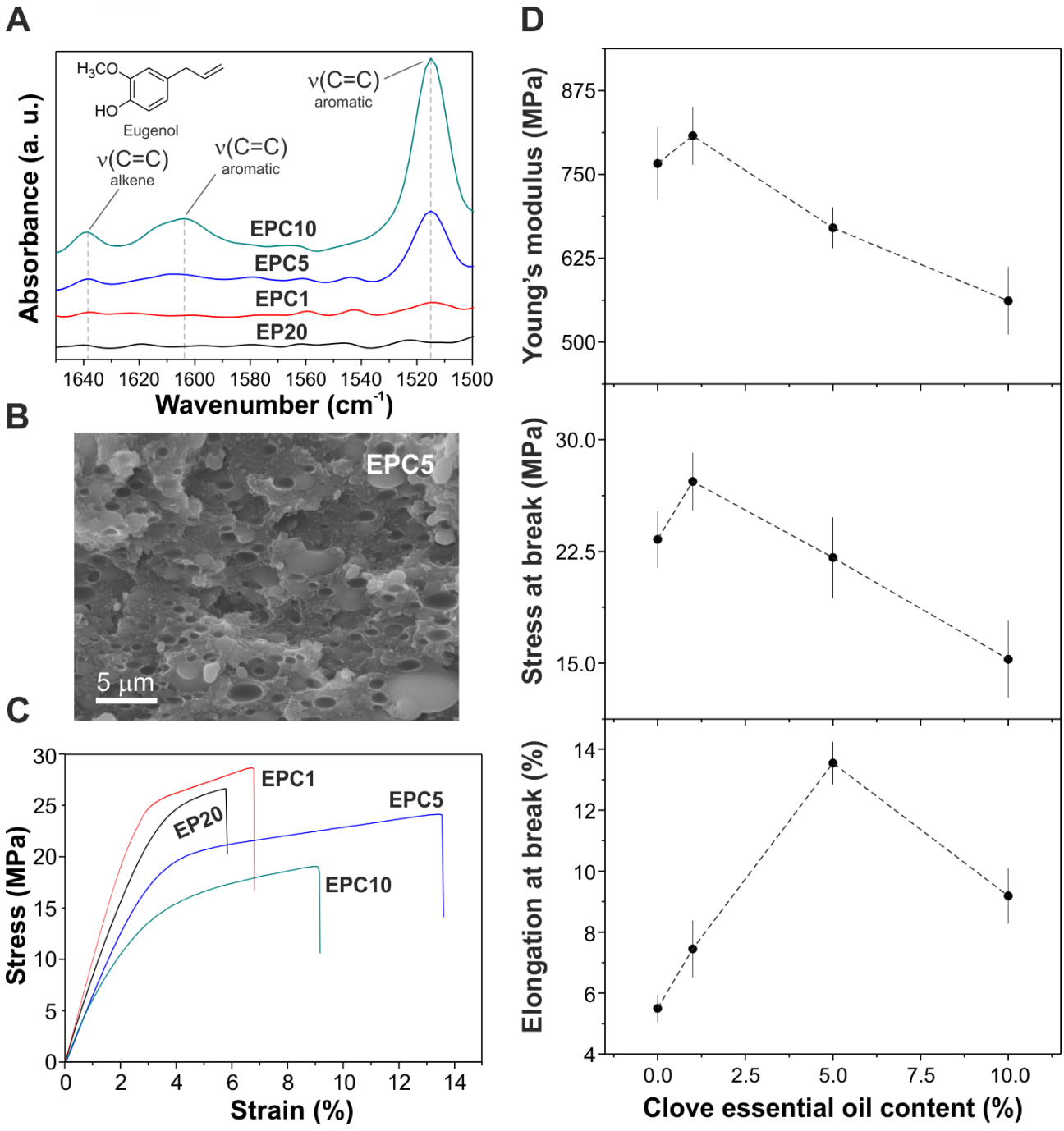

Figure 6. A, ATR-FTIR spectra of EP20, EPC1, EPC5, and EPC10 samples in the 1650-1500 cm^{-1} region. Eugenol chemical structure is included. **B**, compositional SEM cross-section of the EPC5 sample after a tensile test. **C**, representative stress-strain curves of EP20, EPC1, EPC5, and EPC10 samples. **D**, variation of the Young's modulus, stress at break and elongation at break of the EP20 sample with the content of clove essential oil.

The antioxidant and antimicrobial properties of the composites with clove essential oil are reported in Figure 7. Figure 7A shows the results for the radical scavenging activity (RSA) of EP20, EPC1, EPC5, and EP10 samples determined by using DPPH• method. EP20 displayed a final value of RSA

close to 10% after 1.5 h of measurement. The antioxidant properties of the composites with clove essential oil were much higher, eventually reaching 100% RSA after 1.5 hours. On the other hand, phenolic compounds present in the clove essential oil can denature proteins and react with cell membrane phospholipids changing their permeability and inhibiting a great number of Gram-negative and Gram-positive bacteria as well as different types of yeast (Chaieb et al., 2007; Walsh et al., 2003). The biofilm inhibition assay was performed against *E. coli*, *S. aureus*, and *P. aeruginosa*. They are common pathogens that can be easily found in foods and are responsible for many foodborne illnesses (Franzetti & Scarpellini, 2007; Law, Ab Mutalib, Chan, & Lee, 2014; Scallan et al., 2011). Figure 7B-D shows *E. coli*, *S. aureus* and *P. aeruginosa* biofilm formation on EP20 and EPC5 composite materials. The bacterial population of *E. coli* and *P. aeruginosa* decreased with time in both substrates, while the population of *S. aureus* was similar at 24 h and 48 h. Furthermore, the average values of OD at 540 nm for EP20 were higher than those of EPC5. In particular, biofilm formation by *E. coli* was significantly inhibited in the presence of clove essential oil both at 24 h and 48 h ($0.001<p<0.01$ and $p<0.0001$, respectively). In this case, a percentage of biofilm inhibition of ~44% at 24 h and ~57% at 48 h was calculated. Biofilm formation by *S. aureus* was not significantly inhibited at 24 h, but the inhibition became significant at 48 h ($0.001<p<0.01$), with a percentage of biofilm inhibition of ~62%. Finally, the biofilm formation by *P. aeruginosa* was significantly inhibited only at 24 h ($p<0.05$) with a percentage of inhibition of ~38%. These results confirm the good antimicrobial properties of the films incorporating clove essential oil.

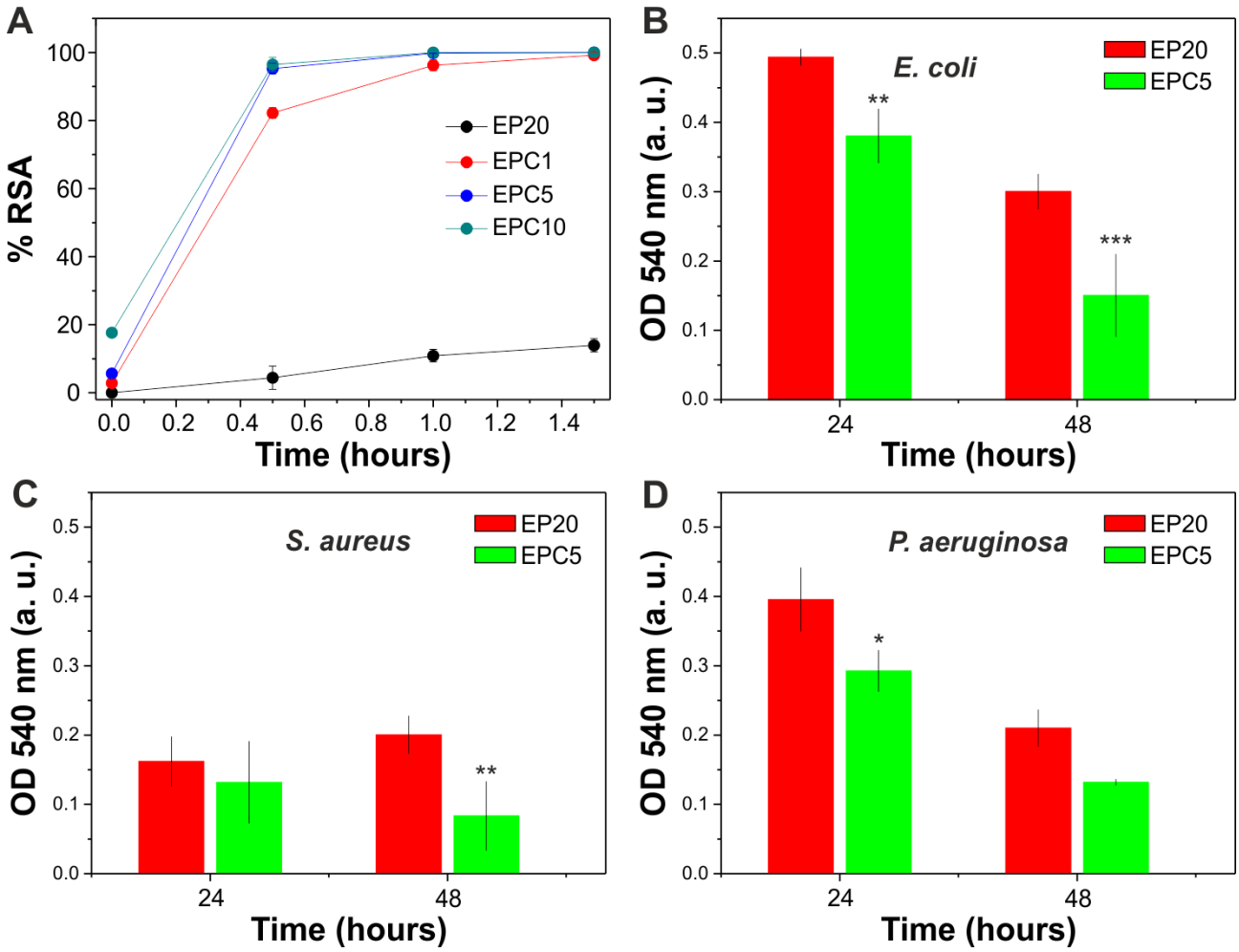

Figure 7. A, antioxidant capacity of EP20, EPC1, EPC5, and EPC10 samples. **B**, **C**, **D**, biofilm inhibition effect of EP20 and EPC5 samples at 24 and 48 h against *E. coli*, *S. aureus*, and *P. aeruginosa*, respectively. Optical density is proportional to the bacterial population. The means ± S.D. for 5 replicate wells are reported (*$p<0.05$, **$0.001<p<0.01$, ***$p<0.001$ *vs.* EP20 group).

4.- Conclusions

The properties of ethyl cellulose films can be tuned by the addition of relatively low amounts of (5-20 wt.%) of PDMS. When ethyl acetate solutions of both components are blended and drop-casted, self-standing films made of EC-rich matrices and PDMS-rich particles are formed. The density and diameter of the particles increase with the PDMS content. There is also an interaction through H-bonds between the two polymers, as confirmed by ATR-FTIR spectroscopy. All these phenomena affect the final characteristics of the composites. The opacity, hydrophobicity, and water barrier properties improve significantly with the PDMS content, while tensile mechanical properties are reduced. The addition of low percentages of clove essential oil does not affect the morphology of the composite, but improves the flexibility of the material. Moreover, the presence of clove essential oil

considerably increases the antioxidant properties of the composite and can inhibit the growth of common pathogens. In view of the results, the polymeric composite formed by 80 wt.% EC, 20 wt.% PDMS and an additional 5.0 wt.% clove essential oil can be a future candidate as a smart food packaging material.

References

Badulescu, R., Vivod, V., Jausovec, D., & Voncina, B. (2008). Grafting of ethylcellulose microcapsules onto cotton fibers. *Carbohydrate Polymers,* 71(1), 85-91.

Biji, K. B., Ravishankar, C. N., Mohan, C. O., & Srinivasa Gopal, T. K. (2015). Smart packaging systems for food applications: a review. *Journal of Food Science and Technology,* 52(10), 6125-6135.

Brandwilliams, W., Cuvelier, M. E., & Berset, C. (1995). USE OF A FREE-RADICAL METHOD TO EVALUATE ANTIOXIDANT ACTIVITY. *Food Science and Technology-Lebensmittel-Wissenschaft & Technologie,* 28(1), 25-30.

Burt, S. (2004). Essential oils: their antibacterial properties and potential applications in foods—a review. *International Journal of Food Microbiology,* 94(3), 223-253.

Cerqueira, M. A. P. R., Pereira, R. N. C., da Silva Ramos, O. L., Teixeira, J. A. C., & Vicente, A. A. (2016). *Edible Food Packaging: Materials and Processing Technologies*: CRC Press.

Ceseracciu, L., Heredia-Guerrero, J. A., Dante, S., Athanassiou, A., & Bayer, I. S. (2015). Robust and Biodegradable Elastomers Based on Corn Starch and Polydimethylsiloxane (PDMS). *ACS Applied Materials & Interfaces,* 7(6), 3742-3753.

Chaieb, K., Hajlaoui, H., Zmantar, T., Kahla-Nakbi, A. B., Rouabhia, M., Mahdouani, K., & Bakhrouf, A. (2007). The chemical composition and biological activity of clove essential oil, Eugenia caryophyllata (Syzigium aromaticum L. Myrtaceae): a short review. *Phytotherapy Research,* 21(6), 501-506.

Chan, L. W., Ong, K. T., & Heng, P. W. S. (2005). Novel Film Modifiers to Alter the Physical Properties of Composite Ethylcellulose Films. *Pharmaceutical Research,* 22(3), 476-489.

Chattopadhyay, P., Dhiman, S., Borah, S., Rabha, B., Chaurasia, A. K., & Veer, V. (2015). Essential oil based polymeric patch development and evaluating its repellent activity against mosquitoes. *Acta Tropica,* 147, 45-53.

Chowdhry, B. Z., Ryall, J. P., Dines, T. J., & Mendham, A. P. (2015). Infrared and Raman Spectroscopy of Eugenol, Isoeugenol, and Methyl Eugenol: Conformational Analysis and Vibrational Assignments from Density Functional Theory Calculations of the Anharmonic Fundamentals. *The Journal of Physical Chemistry A,* 119(46), 11280-11292.

Davidovich-Pinhas, M., Barbut, S., & Marangoni, A. G. (2014). Physical structure and thermal behavior of ethylcellulose. *Cellulose,* 21(5), 3243-3255.

de Brabander, C., van den Mooter, G., Vervaet, C., & Remon, J. P. (2002). Characterization of ibuprofen as a nontraditional plasticizer of ethyl cellulose. *Journal of Pharmaceutical Sciences,* 91(7), 1678-1685.

Elzein, T., Galliano, A., & Bistac, S. (2004). Chains anisotropy in PDMS networks due to friction on gold surfaces. *Journal of Polymer Science Part B: Polymer Physics,* 42(12), 2348-2353.

Esteves, A. C. C., Brokken-Zijp, J., Laven, J., Huinink, H. P., Reuvers, N. J. W., Van, M. P., & de With, G. (2009). Influence of cross-linker concentration on the cross-linking of PDMS and the network structures formed. *Polymer,* 50(16), 3955-3966.

Franzetti, L., & Scarpellini, M. (2007). Characterisation ofPseudomonas spp. isolated from foods. *Annals of Microbiology,* 57(1), 39-47.

Gupta, V., Singh, S., Srivarstava, M., Ahmad, H., Pachauri, S. D., Khandelwal, K., . . . Dwivedi, A. K. (2016). Effect of polydimethylsiloxane and ethylcellulose on in vitro permeation of centchroman from its transdermal patches. *Drug Delivery,* 23(1), 113-122.

Hammer, C. F. (1978). *Chapter 17 - Polymeric Plasticizers A2 - PAUL, D.R*. In S. Newman (Ed.), *Polymer Blends* (pp. 219-241): Academic Press

Heredia-Guerrero, J. A., Benítez, J. J., Cataldi, P., Paul, U. C., Contardi, M., Cingolani, R., . . . Athanassiou, A. (2017). All-Natural Sustainable Packaging Materials Inspired by Plant Cuticles. *Advanced Sustainable Systems,* 1(1-2), 1600024-n/a.

Ho, T. T. T., Zimmermann, T., Ohr, S., & Caseri, W. R. (2012). Composites of Cationic Nanofibrillated Cellulose and Layered Silicates: Water Vapor Barrier and Mechanical Properties. *Acs Applied Materials & Interfaces,* 4(9), 4832-4840.

Hyppölä, R., Husson, I., & Sundholm, F. (1996). Evaluation of physical properties of plasticized ethyl cellulose films cast from ethanol solution Part I. *International Journal of Pharmaceutics,* 133(1), 161-170.

Iqbal, H. M. N., Kyazze, G., Locke, I. C., Tron, T., & Keshavarz, T. (2015). Poly(3-hydroxybutyrate)-ethyl cellulose based bio-composites with novel characteristics for infection free wound healing application. *International Journal of Biological Macromolecules,* 81(Supplement C), 552-559.

Jamuna, P. (2010). Evaluation of certain food additives. Sixty-ninth report of the Joint FAO/WHO Expert Committee on Food Additives (JECFA). WHO Technical Report Series No. 952. 2009. World Health Organization. Geneva, pages 208. Springer.

Kwiatkowski, P., Giedrys-Kalemba, S., Mizielińska, M., & Bartkowiak, A. (2016). Modification of PLA foil surface by ethylcellulose and essential oils. *Journal of Microbiology, Biotechnology and Food Sciences,* 5(5), 440-444.

Laredo, T., Barbut, S., & Marangoni, A. G. (2011). Molecular interactions of polymer oleogelation. *Soft Matter,* 7(6), 2734-2743.

Law, J. W.-F., Ab Mutalib, N.-S., Chan, K.-G., & Lee, L.-H. (2014). Rapid methods for the detection of foodborne bacterial pathogens: principles, applications, advantages and limitations. *Frontiers in Microbiology,* 5, 770.

Lu, H., Wang, Q., Li, G., Qiu, Y., & Wei, Q. (2017). Electrospun water-stable zein/ethyl cellulose composite nanofiber and its drug release properties. *Materials Science and Engineering: C,* 74(Supplement C), 86-93.

Lukasiak, J., Dorosz, A., Prokopowicz, M., Rosciszewski, P., & Falkiewicz, B. (2005). *Biodegradation of Silicones (Organosiloxanes)*. In *Biopolymers Online*: Wiley-VCH Verlag GmbH & Co. KGaA

Mashak, A., & Rahimi, A. (2009). Silicone Polymers in Controlled Drug Delivery Systems: A Review. *Iranian Polymer Journal,* 18(4), 279-295.

Matan, N., Rimkeeree, H., Mawson, A. J., Chompreeda, P., Haruthaithanasan, V., & Parker, M. (2006). Antimicrobial activity of cinnamon and clove oils under modified atmosphere conditions. *International Journal of Food Microbiology,* 107(2), 180-185.

Murtaza, G. (2012). Ethylcellulose microparticles: a review. *Acta Poloniae Pharmaceutica - Drug Research,* 69(1), 11-22.

Patil, D. K., Agrawal, D. S., Mahire, R. R., & More, D. H. (2016). Synthesis, characterization and controlled release studies of ethyl cellulose microcapsules incorporating essential oil using an emulsion solvent evaporation method *American Journal of Essential Oils and Natural Products,* 4(1), 23-31.

Rahman, M., & Brazel, C. S. (2004). The plasticizer market: an assessment of traditional plasticizers and research trends to meet new challenges. *Progress in Polymer Science,* 29(12), 1223-1248.

Scallan, E., Hoekstra, R. M., Angulo, F. J., Tauxe, R. V., Widdowson, M.-A., Roy, S. L., . . . Griffin, P. M. (2011). Foodborne Illness Acquired in the United States—Major Pathogens. *Emerging Infectious Diseases,* 17(1), 7-15.

Shogren, R. (1997). Water vapor permeability of biodegradable polymers. *Journal of environmental polymer degradation,* 5(2), 91-95.

Tran, T. N., Athanassiou, A., Basit, A., & Bayer, I. S. (2017). Starch-based bio-elastomers functionalized with red beetroot natural antioxidant. *Food Chemistry,* 216, 324-333.

Tran, T. N., Heredia-Guerrero, J. A., Mai, B. T., Ceseracciu, L., Marini, L., Athanassiou, A., & Bayer, I. S. (2017). Bioelastomers Based on Cocoa Shell Waste with Antioxidant Ability. *Advanced Sustainable Systems*, 1700002-n/a.

Walsh, S. E., Maillard, J. Y., Russell, A. D., Catrenich, C. E., Charbonneau, D. L., & Bartolo, R. G. (2003). Activity and mechanisms of action of selected biocidal agents on Gram-positive and -negative bacteria. *Journal of Applied Microbiology,* 94(2), 240-247.

461 Wüstenberg, T. (2014). *Ethylcellulose*. In T. Wüstenberg (Ed.), *Cellulose and Cellulose Derivatives in the Food*
462 *Industry* (pp. 275-318): Wiley-VCH Verlag GmbH & Co. KGaA
463 Zahid, M., Heredia-Guerrero, J. A., Athanassiou, A., & Bayer, I. S. (2017). Robust water repellent treatment
464 for woven cotton fabrics with eco-friendly polymers. *Chemical Engineering Journal,* 319, 321-332.

465